wisconsin astrophysics

The Io Sulfur Torus in 1981

by

Ronald J. Oliversen[1,3]

Frank Scherb[2,3]

and

Fred L. Roesler[2,3]

NUMBER 249

September 1986

[1]Laboratory for Astronomy and Solar Physics, NASA/Goddard Space Flight Center, Code 684, Greenbelt, MD 20771

[2]University of Wisconsin, Department of Physics, Madison, WI 53706

[3]Visiting Astronomer, Kitt Peak National Observatory, National Optical Astronomy Observatories which is operated by the Association of Universities for Research in Astronomy, Inc., under contract with National Science Foundation

09/11/86

The Io Sulfur Torus in 1981

by

Ronald J. Oliversen[1,3], Frank Scherb[2,3], and Fred L. Roesler[2,3]

[1]Laboratory for Astronomy and Solar Physics, NASA/Goddard Space Flight Center, Code 684, Greenbelt, MD 20771

[2]University of Wisconsin, Department of Physics, Madison, WI 53706

[3]Visiting Astronomer, Kitt Peak National Observatory, National Optical Astronomy Observatories which is operated by the Association of Universities for Research in Astronomy, Inc., under contract with National Science Foundation.

Submitted to Icarus

Pages 40 including

Tables 4 and

Figures 9

ABSTRACT

A Fabry-Perot/CCD spectrometer was used to obtain images of the Io torus in emission lines of [S II] λ6716, λ6731 and [S III] λ9531 in 1981 February and March on the 2.1-meter telescope at KPNO. The [S II] and [S III] images showed a large variation in brightness and radial extent. There is an indication that [S II] and [S III] emissions in the warm torus are correlated. The [S II] and [S III] emissions in the warm torus also have similar scale heights along the magnetic field lines of ~0.6 R_J - 0.72 R_J. The east-west asymmetry in the [S II] images taken at similar magnetic longitudes, but 2.5 Jovian rotations apart, supports the theory of convective motions suggested by others. In addition to the images, simultaneous measurements of the [S II] λ6731 line profile were also made on one night using a Fabry-Perot scanning spectrometer on the 4-meter at KPNO. The [S II] spectral scans implied ion temperatures of $(52\pm10)\times10^3$ K at 5.2 R_J to 5.6 R_J from Jupiter and a minimum temperature of at least 3×10^5 K at 6 R_J from Jupiter.

I. INTRODUCTION

The 1979 *in situ* observations of the Io torus by Voyager I and the long-range monitoring of the warm torus by the ultraviolet spectrometers (UVS) of Voyager I and II (Sandel and Broadfoot, 1982a) have often been used to characterize the torus and serve as a model to which other observations are compared. The Voyager I plasma science experiment PLS (Bagenal and Sullivan 1981) determined that the torus could be divided into at least two distinct regions; a cold, inner torus with ion temperatures T_i of a few eV, and a warm outer torus with ion temperatures at least an order-of-magnitude hotter. Several ground-based investigations (Morgan 1985a; Pilcher and Morgan 1980; Trafton 1980; Trauger *et al.* 1980) have demonstrated the correlation of [S II] emission in the cold torus with Jovian magnetic longitude λ_{III}(1965). The brightest [S II] emission occurred in the 'active sector' - the range of magnetic longitudes (175^{o}-320^{o}) over which Io is known to modulate the Jovian decametric radiation (Carr and Desch 1976; Dessler and Hill 1979). In contrast to the ground-based [S II] measurements, the UVS experimenters found the S^{+2} ions in the warm torus were uncorrelated with Jovian magnetic longitude (Sandel and Broadfoot 1982a). Instead, Sandel and Broadfoot (1982b) detected a local time or east-west asymmetry in the UVS data which they attributed to changes in electron temperature T_e. More recently, Morgan (1985a) has reported a similar east-west asymmetry in his optical data. However, it is unclear how the optical asymmetry is related to the UV asymmetry since the optical emissions would be insensitive to changes in T_e (Shemansky 1980).

Although the Voyager spacecraft supplied the most detailed data on physical conditions in the torus, the spatial and temporal coverage was

limited. The ground-based observations of the torus cover several years, but the use of different instruments with different fields of view, monitoring the torus at 'random' times, and using different methods of intensity calibration has impeded ground-based observers from deriving their own 'standard' model of the torus. Morgan (1985a) has overcome some of these difficulties by collecting extensive, high quality, calibrated spectrographic data over a 4 month period in 1981 from February to May and developing a three-dimensional model (Morgan 1985b) to describe the average conditions within the torus at that observational epoch. He supplemented this database to refine his model by including contemporaneous observations of Brown and Shemansky (1982), Oliversen (1983), Trauger (1984), and Pilcher *et al.* (1985). Morgan's model differs from the Voyager picture of the torus in several respects: (1) the decrease in mixing ratios with increasing distance starts at smaller radii; (2) the outer torus densities are 1.5 to 2 times higher; and (3) the outer torus ion temperatures are a factor of 2 cooler. Morgan's model also demonstrates that density changes caused by convective motion, as suggested by Barbosa and Kivelson (1983) and Ip and Goertz (1983), are adequate to explain the east-west asymmetry reported by Morgan (1985a).

The data presented here are described in more detail in Oliversen (1983), but more recent improvements in the intensity calibration and instrumental characteristics are included in this paper. These data alone are insufficient to distinguish between temporal and spatial variations, and therefore are best viewed in the context of other Io torus data taken in 1981 and the 1981 model of Morgan (1985b) who used our data to help formulate his model.

II. OBSERVATIONS

As part of an ongoing program to study the spatial and temporal variation of the torus, we took images of the torus in the emission lines of [S II] λ6716, λ6731 and [S III] λ9531 in 1981 February and March with a Fabry-Perot/CCD (FP/CCD) imaging spectrometer on the 2.1 meter telescope at Kitt Peak National Observatory (KPNO). This type of direct imagery at low spectral resolution is useful for investigating the morphology and intensity structure of the torus, as is evident from [S II] and [S III] images first obtained by Pilcher (1980) and Roesler et al. (1982), respectively, and more recently by Trauger (1984) and Pilcher et al. (1985).

On 1981 March 26 we succeeded in measuring the [S II] λ6731 emission line profiles using a scanning Fabry-Perot spectrometer mounted at the Cassegrain focus of the KPNO 4-meter telescope while simultaneously obtaining [S II] torus images on the KPNO 2.1-meter telescope. The high spectral resolution line profile provides a direct measurement of the perpendicular ion temperature[1], whereas, low spectral resolution torus images provide indirect information on the parallel ion temperatures by applying models to the observed spatial distributions. The simultaneity of the measurements is important for interpreting the spatial distribution of the ions since the torus can change rapidly.

The FP/CCD instrumentation and method of operation are similar to that described by Roesler et al. (1982), with more detailed information given by Oliversen (1983). Different Fabry-Perots were used in February and March; their wavelength dependent passbands are listed in Table I. The detector was

[1]To first order the Earth can be considered in the Jovian equatorial plane, thus our line-of-sight is approximately perpendicular to the Jovian magnetic field.

an RCA 512x320 pixel CCD camera operating in a 2x2 prebinning mode which corresponded to an image scale of 2.64 "/'binned pixel' (or 0.125 R_J/pixel in February and 0.119 R_J/pixel in March). The CCD camera system is described in detail by York et al. (1981).

Despite the faintness of the torus emission, our observational approach obtained short (~10 min) exposures which ensured the rotation and aspect wobble of the torus would not seriously smear each image. The catalog of our emission line images is given in Table II. Continuum images, obtained with the FP tuned several Angstroms away from the Doppler-shifted emission and avoiding solar absorption features, were taken on the torus either before or after each emission line image. The image of Jupiter, located on an occulting mask in the focal plane of the telescope, was the guide object. Guiding was accurate to 2"-3" (0.1-0.15 R_J) with the greater uncertainty being associated with observations made to the east of Jupiter. Three to five separate images of Jupiter were also taken each night to define the spatial relation between Jupiter and the torus, and to provide an intensity calibration.

Unfortunately, the CCD camera shutter was erratic for exposures less than 1 second, making the Jovian intensity calibrations unreliable. Therefore, a more indirect method of absolute intensity calibration was required. The intensity calibrations for March 26 were determined from a series of [S II] and [S III] images of the planetary nebula NGC 2392, effectively scanning the nebular emission lines. Each datum in these low resolution line profile 'scans' was determined by integrating the signal over the entire nebula. To correct for any flux which may have been missed in these limited scans, the scans were compared to high resolution line profiles of the entire nebula (Scherb, Oliversen, and Roesler unpublished data) convolved with the instrumental profile. The resultant NGC 2392 flux corrections were 25% for

[S II] and 10% for [S III]. The NGC 2392 total [S II] doublet flux is 4.7×10^{-12} ergs cm^{-2} s^{-1} (O'Dell 1963) with a doublet ratio (F_{6731}/F_{6716}) of 0.61 (Aller and Epps 1976). The NGC 2392 [S III]λ9531 flux is 4.27×10^{-11} ergs cm^{-2} s^{-1} (Collins et al. 1961).

The intensity calibrations for February 16 and March 25 were determined by comparing the scattered light intensities in the torus continuum images taken on those nights with continuum images taken on March 26. The spatial variation of the scattered light from Jupiter clearly indicates the scattering is caused by the telescope optics. Thus scattering should be constant over several nights in the absence of serious problems, such as condensation on the mirrors, allowing reasonably accurate relative calibration between nights. An additional comparison was made between images of the Trapezium in NGC 1976 taken on February 16 and March 25 in the continuum near the [S II] lines. We concluded that the combined system and sky transmittance was lower by 40% in February and comparable between nights in March. Overall, we believe the relative intensity calibration consistency is within ~10-15% during and between nights in March and consistent to within ~30% between months.

The absolute intensity calibration depends on the accuracy of the NGC 2392 fluxes. A rough estimate of the accuracy of our intensities was made by comparing our images to low resolution slit spectra (Morgan 1985a) taken at approximately the same Jovian longitude, on the same side of Jupiter, and within 1 to 5 days of our observations. Despite the spatial inhomogeneities and time variations that characterize the torus, the agreement was usually within 50%. However, it should be noted, spectra taken within days of one another by Brown and Shemansky (1982) and Morgan (1985a) disagree in their absolute intensities by a factor of four.

The FP scanning spectrometer on the 4-meter telescope was operated in the Doppler-compensated mode (Trauger and Roesler 1972) with an 18" (0.8 R_J) field of view (FOV) centered 5.2 R_J to 6.0 R_J from Jupiter. The wavelength calibration and velocity resolution (6 km/s) were determined from scans of the thorium I line at λ6729.9325. Guiding was done on the limb of Jupiter and was accurate to <1" (0.05 R_J). The intensity calibration was based on a scan of the planetary nebula NGC 6210 for which the [S II]λ6731 flux is 3.3×10^{-12} ergs cm^{-2} s^{-1} (Dinerstein 1980; Barker 1978). There is a systematic difference in the intensity calibration between the two Fabry-Perots instruments with the 4-meter calibration having the torus ~2 times brighter than the 2-meter calibration. The angular size of NGC 6210 is 20"x13", so our 18" FOV would exclude a small fraction of the nebula and we do not believe centering was a problem. Additional instrumental details are given by Oliversen (1983).

III. DATA REDUCTION

Figure 1 shows examples of raw emission and continuum FP/CCD data frames. Each frame is dominated by scattered continuum light from Jupiter, originating mainly in the telescope and in the instrument. The continuum spatial distribution is complicated by Galilean satellites, cosmic ray interactions in the CCD, and ghost images caused by internal reflections in the optics.

The data reduction process for each emission line image involved subtracting the continuum frame, dividing by the flat field frame and correcting for the position-dependent spectral response of the FP. Ideally, the background contribution in the emission line frame would be completely removed by scaling and subtracting the continuum frame. However, in this

case, a position-dependent residual background remained after the subtraction. There were two possible reasons for this: (1) if the background continuum had spectral structure (e.g., Solar Fraunhofer lines or terrestrial water vapor absorption lines), then, when the FP was tuned to the continuum, this background structure would shift spatially with respect to the continuum in the emission line image; or (2) if the scattered light distribution was sensitively dependent on the position of Jupiter in the focal plane, then the scattered light distribution would vary due to any systematic guiding irregularities.

The residual background in each subtracted image was represented by a grid of intensities empirically determined for every 5 rows (0.60 R_J) by 3 columns (0.36 R_J). The intensities for the other pixels within each subtracted image were interpolated from these grids. The residual background surrounding the sulfur emission was used to estimate the residual background component within the torus image. This residual background was removed from the image over the central 50x35 pixels (6 R_J x 4.2 R_J), thus leaving only sulfur emission and small-scale structure (i.e., Galilean moons, reflections of moons and cosmic ray hits). Small-scale features when identified as moon reflections or cosmic ray hits were removed by fitting them with two-dimensional elliptical Gaussians and then subtracting the model fit.

Finally, with the background continuum removed, the remaining sulfur emission was corrected for the position-dependent spectral response of the FP. The FP transmittance depended on the angle of the incident light, the spectral line profile, and the Doppler-shifted wavelength of the emission line. The spectral line profile was modeled by Gaussians whose widths corresponded to the temperatures of the cold ($5x10^4$) and warm ($5x10^5$) torus. The spectral line center was assumed to be at the corotation Doppler-shifted

wavelength. Figure 2 shows an example of the calculated FP transmittance function (dashed lines) used to produce a final torus image (solid lines). The FP transmittance is calculated relative to the transmittance of the FP to a very narrow emission line with any absolute transmission losses through the FP being corrected in the intensity calibration. The effect of the finite spectral line width on the calculated FP transmittance was $\sim$<3% for the February torus images and $\sim$<10% for the March images.

The quality of a final image depends on the completeness of the background subtraction and the accuracy of the FP transmission correction. Except for a few small unidentifiable features ($\sim$2-3 pixels), we believe the background subtraction is good. The calculated FP transmission is most sensitive to the position of the torus with respect to the FP 'ring pattern' (Fig. 2) and the assumption that the line central wavelength is given by strict corotation. For example, if the torus were lagging behind the corotational speed, then for observations to the west (east) of Jupiter the FP 'ring pattern' would be expanded (contracted). In particular, for Fig. 2a if the torus were assumed to have a 5% corotational lag then the ring diameter at the peak transmittance would increase from 2.25 R_J to 2.50 R_J and the central transmittance would decrease from 0.82 to 0.76. Likewise, for Fig. 2b the ring diameter would increase from 1.38 R_J to 1.88 R_J and the central transmittance would decrease from 0.96 to 0.95. Therefore, we have assigned a quality factor (Table II) to each image to reflect the degree to which the image may be affected by systematic errors.

The data reduction for each 4-meter FP spectral scan involved a least-squares fit to the line profile of a Gaussian function convolved with the instrumental response function (Fig. 3). The sloping background was due to the wavelength dependence of the interference filter transmission. The 4-

meter FOV was inadvertently displaced systematically north of the centrifugal equator (Fig. 4) due to an error of using an incorrect value for the angle on the sky between the celestial equator and the Jovian spin equator. Thus, the measured torus brightness and predicted corotational velocities of these scans depended on the distance from Jupiter and the centrifugal latitude of the FOV.

IV. RESULTS

Figure 5 shows a sample of our images which represent the variations detected in [S II] and [S III] intensities and spatial distributions. The [S II] intensity maxima were generally located at 5.0 to 5.6 R_J from Jupiter (Fig. 6a) with a peak [S II] intensity variation of a factor ~4 (Table II). The maximum detectable radial extent was highly variable for the [S II] emission (Fig. 6a), ranging from near Io's orbit (5.9 R_J) to ~7.3 R_J, nearly as far as the farthest [S III] emission. In comparison, the [S III] intensity maxima were located at 5.65 to 5.95 R_J from Jupiter (Fig. 6b) with a peak intensity variation from 230 R to 630 R. The most distant detectable [S III] emission occurred from 6.65 to 7.45 R_J (Fig. 6b). Also, for comparison, Fig. 6 shows the results from the 1980 torus data of Roesler et al. (1982). This wide range of variation in peak position, intensity and radial extent is consistent with numerous other observations (Pilcher et al. 1985; and reviews by Pilcher and Strobel (1983); Brown et al. 1983; and references therein).

The extension of the emission along the magnetic field can be used to obtain some information on the energy distribution of the ions parallel to the field lines in the plasma frame of reference. We evaluated the intensity distribution along the magnetic field lines for images whose lines-of-sight were approximately at constant Jovian centrifugal latitudes ('edge-on') using

the thermal model of the torus by Hill and Michel (1976) as modified by Bagenal and Sullivan (1981). In this model, the density n(s) of a Maxwellian plasma as a function of distance s from the centrifugal symmetry plane along a magnetic field line is given by

$$n(s) = n_o \exp(-(s/H)^2)$$

where n_o is the density in the symmetry plane, and H, the centrifugal scale height, is given by

$$H = \left(\frac{T_i}{28400\ m_i^*}\right)^{1/2} \quad (R_J) \qquad (1)$$

where T_i is the ion temperature in the direction along the field line and m_i^* is the effective ion mass (amu) (Bagenal and Sullivan 1981).

According to the model, the intensity distribution along a field line should have a Gaussian profile with scale height H. Figure 7 shows for a [S III] 'edge-on' image the results of a least-squares fit of a Gaussian profile convolved with the image point-spread function as a function of magnetic L-shell (magnetic field line equatorial crossing distance using the offset tilted dipole model of Smith et al. (1976)). The results of the Gaussian scale height analysis for images that are approximately 'edge-on' are shown in Fig. 8. The [S II] and [S III] scale heights in the warm torus ($L \geq 5.8$ R_J) were similar during the same epoch and approximately constant with L-shell. The [S II] and [S III] scale heights (Table III) for February were 0.72 ± 0.04 R_J and 0.73 ± 0.03 R_J, respectively, and the scale heights for March

were 0.58±0.06 R_J and 0.62±0.04 R_J, respectively. Trauger (1984) also reported [S II] and [S III] to have similar scale heights varying from 0.6 to 0.8 R_J for images taken during the 1981 to 1983 apparitions. Also, Fig. 8 shows the results of additional scale height analysis of the 1980 data of Roesler et al. (1982).

We used an azimuthally symmetric model of the warm torus to investigate the effect of aspect wobble on the scale height analysis. The model is similar in form to the one used by Sandel and Broadfoot (1982a) but without the local time asymmetry. The model had an emission rate function (photons cm^{-3} s^{-1}) with a peak at 6.0 R_J, decreasing inward linearly to zero at 5.7 R_J, decreasing outward parabolically to zero at 8 R_J and proportional to $\exp(-(s/H)^2)$ perpendicular to the symmetry plane, where H = 0.70 R_J. The parameters (i.e., radii of inner edge, peak, and outer edge; and scale height) were chosen so that the calculated model produced a projected integrated brightness representative of the February 16 [S III] image obtained at 11:59 UT (Fig. 9). The model is not unique and the azimuthal symmetry is too simple, but it is adequate for studying the different viewing geometries. The model demonstrated that changing the aspect Φ from 0° to 3° only increased the apparent scale height of the images by 0.03 R_J for L≥5.8 R_J. This is consistent with the [S III] images obtained on February 16 at 11:59, 12:28 and 12:42 UT which all yielded similar scale heights as the Jovicentric centrifugal latitude ϕ of the Earth changed from -0.4° to 1.5° to 2.4°, respectively. Also, the model showed that a maximum decrease of only 20% in peak intensity of the warm torus could be attributed to a varying aspect (0° to 9°). A similar effect due to changing aspect was reported for Morgan's 1981 model (Morgan 1985b).

Interpretation of the [S II] scale heights within L=5.8 R_J is complicated when the line-of-sight intersects both warm and cold regions of the [S II] torus. When [S II] emission was not detectable outside of Io's orbit, analysis of the cold [S II] emission yielded scale heights of ~0.2-0.3 R_J (Pilcher 1980; Roesler et al. 1982). However, when [S II] emission was clearly present outside of Io's orbit (Fig. 5), the measured scale height inside of L=5.8 R_J was ~0.4-0.5 R_J (Fig. 8). These scale heights are intermediate between typical scale heights for the cold and warm regions of the torus, and probably reflect a two-component distribution which was smeared out due to the low spatial resolution and data reduction limitations described earlier.

The March 25 and 26 [S II] images were taken at similar magnetic longitudes, but on the west and east sides of Jupiter, respectively. They showed the peak intensity to be systematically farther from Jupiter and slightly fainter (Table II) on the eastern side (Fig. 6a). A similar result was reported by Morgan (1985a) and Pilcher et al. (1985). They noted that the east-west distance difference was in qualitative agreement with the suggestions (Barbosa and Kivelson 1983; Ip and Goertz 1983) that a dawn-to-dusk electric field displaces the ion orbits towards the dawn (east) side. Barbosa and Kivelson (1983) predicted an offset of ~0.18 R_J for an orbit at 6 R_J, leading to an apparent east-west distance difference of 0.35 R_J.

The results from the FP scans of [S II] λ6731 emission are given in Table IV. Each measured spectral line center is shown as the rotational Doppler-shifted velocity in the Jovian reference frame assuming the [S II] rest wavelength is 6730.85 Å (Trauger et al. 1980). The measured velocities were consistently 4±1% smaller than the velocities expected for a corotating plasma. However, the deviations from rigid corotational velocities must be

viewed with caution. There are several possible sources of systematic errors. In particular, the nonuniform distribution of [S II] emission within the 0.8 R_J FOV (Fig. 4) could have shifted the wavelength by approximately -1 to -2 km/s. Also, there could have been systematic telescope pointing errors which may not be revealed since all the data was taken to the east of Jupiter. Nevertheless, our results are reasonably consistent with those from the Voyager I PLS experiment which directly measured the ion velocities inside of 5.3 R_J to be within 1% of the expected corotational velocity (Bagenal 1985). Furthermore, the PLS data from 5.3 R_J to 5.9 R_J suggest a typical lag of 1-3% behind rigid corotation, with occasional deviations from corotation up to 5% (Bagenal 1985). If our measured line width is assumed to be a thermal width, then the S^+ ion temperature perpendicular to the magnetic field at 5.2 to 5.6 R_J was $(52\pm10)\times10^3$ K (Table IV). This is consistent with both ground-based and Voyager observations of this region of the torus (Trauger et al. 1980; Bagenal 1985).

V. DISCUSSION

The sequences of [S II] images taken on 1981 February 16 and March 25 revealed that the maximum radial extent of the [S II] torus increased from $\sim$6 R_J to $\sim$7 R_J within 70°-90° of longitude, accompanied by an increasing peak brightness (Fig. 6a; Table II). This behavior is similar to that reported by Pilcher et al. (1985) who obtained more extensive longitudinal coverage with [S II] images taken mainly on 1981 March 13 and April 11. In particular, they report [SII] λ6731 intensity peaks at longitudes 180° and 280°, and a broad longitude range of much fainter emission located between ~0° and ~130° on March 13 and between $\sim$350° and $\sim$70° on April 11. They suggest that the peak intensity variations with magnetic longitude and the approximately uniform electron

distribution at this epoch (Brown and Shemansky 1982; Morgan 1985a) can be explained by plasma formation near λ_{III}~180° and 280° with source widths in longitude of 50°-70° and 30°-50°, respectively, and departures from rigid corotation. Our longitudinal coverage is limited, but our March [SII] data are consistent with their data. The [SII] image obtained at λ_{III}=178° (Fig. 5c) was 2-3 times brighter and much more extended than the [SII] images obtained at magnetic longitudes between 345° and 154°. This bright, 'edge-on' [S II] image was also used by Morgan (1985b) to help constrain his model.

Pilcher et al. (1985) predicted that the S III longitudinal distribution at the time of their [S II] observations would have been substantially more uniform, exhibiting weak peaks displaced toward higher longitudes from those of S II. This prediction cannot be confirmed with the single [S III] image taken by us in March. However, this does not appear to describe the torus shown in our February [S III] images. The [S III] images from magnetic longitudes 263° to 65° showed an increase in radial extent from 6.6 R_J to 7.3 R_J (Fig. 6b) and a factor of 2 increase in the peak brightness (Fig. 5d,e; Table II) over a longitudinal range where Pilcher et al. (1985) would have predicted a decrease in peak brightness.

Likewise, the February [S II] images showed a longitudinal asymmetry in radial extent and a 20% increase in peak brightness between magnetic longitudes 286° to 14° (Fig. 6a,b; Table II). The onset of the extended [S II] emission region (λ_{III}=14°) was displaced at least 130° in longitude from the extended region of Pilcher et al. (1985), and in our March data.

The increase in radial extent and brightness of both the [S II] and [S III] emissions implies an increase in plasma mass rather than a change in T_e since the optical emissivities are insensitive to changes in T_e in the warm

torus (Shemansky 1980). Also, there have been other observations indicating the [S II] emission is strongly correlated with the [S III] emission (Roesler et al. 1984; Trauger 1984). Pilcher et al. (1985) have suggested that the [S II] and [S III] emissions are correlated in the absence of significant departures from corotation. However, their suggestion that the plasma is produced locally near magnetic longitudes 180° and 280° does not explain our February images.

The observed scale heights can be used to estimate the ion temperature parallel to the magnetic field if one knows the effective ion mass m_i^*. For a single-component Maxwellian plasma, m_i^* can be expressed as

$$m_i^* = \frac{m_i \left(\frac{T_i}{T_e}\right)}{Z_i + \left(\frac{T_i}{T_e}\right)} \qquad (2)$$

where m_i is the true ion mass, and Z_i is the ion charge state. A range of ion temperatures was obtained from the measured scale heights by assuming: (1) $T_i \gg T_e$, which gives $m_i^* \cong m_i$; and (2) $T_i = T_e$, which gives $m_i^* = m_i/(Z_i+1)$. The results are shown in Table III.

The validity of equation (2) depends on the assumption that m_i^* is constant along a given field line, which is correct if the composition is constant (i.e., if a single ionic species predominates or if most of the ions have similar scale heights). This assumption may not hold in the torus; for example, Morgan and Pilcher (1982) and Bagenal and Sullivan (1981) have reported that [OII] emission has a larger scale height than [S II] emission. However, for the present, we conclude that the ion temperatures are in the range quoted in Table IV, since the [S II] and [S III] emissions have comparable

scale heights. Furthermore, the ion temperatures are probably closer to the upper limits in Table 4, since $T_i \gg T_e$ in the warm torus (Brown et al. 1982, and references therein). In either case, the ion temperatures are cooler than those reported by the Voyager PLS experiment (Bagenal and Sullivan 1981).

Simultaneous acquisition of [S II] images and line profile measurements would provide information on the ion energy distributions both parallel and perpendicular to the magnetic field. However, in our case, the lack of 'edge-on' images on March 26 makes a comparison between the parallel and perpendicular energy distributions difficult. Nevertheless, some conclusions are possible. A scale height analysis of the least 'opened' [S II] image, obtained at 07:50 UT (Fig. 4a), yields an upper limit for H of 0.65 R_J at 6.0 R_J, which implies $T_i < 3.8 \times 10^5$ K parallel to the magnetic field. Using our simple model of the warm torus, we calculate an overestimation of ~0.06 R_J for the scale height at this aspect. Thus the apparent [S II] scale heights to the east and west of Jupiter during March agree. This [S II] image and scan 1 (Fig. 3) were obtained simultaneously, and the apparent lack of a ~150 Rayleigh emission line in scan 1 is explained by having a sufficiently broad emission line. We estimate the line width must be at least 20 km/s to produce the observed profile. This implies a minimum temperature perpendicular to the magnetic field of 3×10^5 K. Thus, there is a possible direct indication that the S^+ ion energy distributions parallel and perpendicular to the magnetic field were identical in the warm torus. This is still a tentative result, and clearly more simultaneous images and line profiles are necessary to clarify this important question about the ion energy distribution in the torus.

ACKNOWLEDGEMENTS

We thank P. M. Ogden, K. Jaehnig, and J. Lattis for their help in building the spectrometers and assisting in the observations. We thank D. G. York and E. B. Jenkins for loaning us the CCD camera system and keeping it operational. We also appreciated the efforts of the KPNO staff for their able assistance at getting visitor's instruments to perform successfully on the 2.1-meter and 4-meter telescopes. RJO is deeply grateful for the constructive comments, criticism and patience of the co-authors during the writing of the dissertation upon which this paper is based. RJO is very appreciative of the support and long discussions with N. A. Oliversen and J. R. Benada III which enabled this work to come to completion. RJO also thanks J. M. Hollis and the Laboratory for Astronomy and Solar Physics, NASA/Goddard Space Flight Center for their assistance while he was a NAS-NRC research associate. This work was supported in part by NSF contracts ATM 8021064, NASA grants 50-002-162 and NAGW-695,and the NAS-NRC associateship program.

REFERENCES

Aller, L. H., and H. W. Epps (1976). Electron densities in gaseous nebula. Astrophys. J., 204, 445-451.

Bagenal, F. (1985). Plasma Conditions inside Io's Orbit: Voyager Measurements. J. Geophys. Res., 90, 311-324.

Bagenal, F., and J. D. Sullivan (1981). Direct plasma measurements in the Io torus and inner magnetosphere of Jupiter. J. Geophys. Res., 86, 8447-8466.

Barbosa, D. D., and M. G. Kivelson (1983). Dawn-dusk electric field asymmetry of Io plasma torus. Geophys. Res. Lett., 10, 210-213.

Barker, T. (1978). Spectrophotometry of planetary nebulae. I. Physical Conditions. Astrophys. J., 219, 914-930.

Brown, R. A., and D. E. Shemansky (1982). On the nature of SII emission from the Io plasma torus. Astrophys. J., 263, 433-442.

Brown, R. A., C. B. Pilcher, and D. F. Strobel (1983). Spectroscopic studies of Io torus. Physics of the Jovian Magnetosphere, (A. J. Dessler, Ed.), pp. 197-225. Cambridge University Press, Cambridge.

Carr, T. D., and M. D. Desch (1976). Recent decametric and hectometric observations of Jupiter. Jupiter, (T. Gehrels, Ed.), pp. 693-737. University of Arizona Press, Tucson.

Collins II, G. W., C. T. Daub, and C. R. O'Dell (1961). Hβ and [OIII] fluxes from planetary nebulae. Astrophys. J., 133, 471-478.

Dessler, A. J., and T. W. Hill (1979), Jovian longitudinal control of Io-related radio emissions. Astrophys. J., 227, 664-675.

Dinerstein, H. L. (1980). Infrared line measurements and the abundance of sulfur in planetary nebulae. Astrophys. J., 237, 486-490.

Hill, T. W., and F. C. Michel (1976). Heavy ions from the Galilean satellites and the centrifugal distortion of the Jovian magnetosphere. J. Geophys. Res., 81, 4561-4565.

Morgan, J. S. (1985a). Temporal and spatial variations in the Io torus. Icarus, 62, 389-414.

Morgan, J. S. (1985b). Models of the Io torus. Icarus, 63, 243-265.

Morgan, J. S., and C. B. Pilcher (1982). Plasma characteristics of the Io torus. Astrophys. J., 253, 406-421.

O'Dell, C. R. (1963). Photoelectric spectrophotometry of planetary nebulae. Astrophys. J., 138, 1018-1034.

Oliversen, R. J. (1983). The Io Plasma Torus: Its Structure and Sulfur Emission Spectra. Ph.D. Thesis, University of Wisconsin-Madison.

Pilcher, C. B. (1980). Images of Jupiter's sulfur ring. Science, 207, 181-183.

Pilcher, C. B., J. H. Fertel, and J. S. Morgan (1985). [SII] images of the Io torus. Astrophys. J., 291, 377-393.

Pilcher, C. B., and J. S. Morgan (1980). The distribution of [SII] emission around Jupiter. Astrophys. J., 238, 375-380.

Pilcher, C. B., and D. F. Strobel (1982). Emissions from neutrals and ions in the Jovian magnetosphere. Satellites of Jupiter, (D. Morrison, Ed.), pp. 807-945. University of Arizona Press, Tucson.

Roesler, F. L., R. J. Oliversen, F. Scherb, J. Lattis, T. B. Williams, D. G. York, E. B. Jenkins, J. L. Lowrance, P. Zucchino, and D. Long (1982). Fabry-Perot/CCD observations of [S III] and [S II] emissions from the Jupiter plasma torus. Astrophys. J., 259, 900-907.

Roesler, F. L., F. Scherb, and R. J. Oliversen (1984). Periodic intensity variation in [SIII] 9531A emission from the Jupiter plasma torus. Geophys. Res. Letters., 11, 128-130.

Sandel, B. R., and A. L. Broadfoot (1982a). Io's hot plasma torus: A synoptic view from Voyager. J. Geophys. Res., 87, 212-218.

Sandel, B. R., and A. L. Broadfoot, A. L. (1982b). Discovery of an Io-correlated energy source for Io's hot plasma torus. J. Geophys. Res., 87, 2231-2240.

Shemansky, D. E. (1980). Radiative cooling efficiencies and predicted spectra of species of the Io plasma torus. Astrophys. J., 236, 1043-1054.

Smith, E. J., L. Davis, Jr., and D. E. Jones (1976). Jupiter's magnetic field and magnetosphere. Jupiter, (T. Gehrels, Ed.), pp. 788-829, University of Arizona Press, Tucson.

Trafton, L. M. (1980). Jovian SII torus: Its longitudinal asymmetry. Icarus, 42, 111-124.

Trauger, J. T. (1984). The Jovian nebula: A post-Voyager perspective. Science (Washington, D.C.), 226, 337-341.

Trauger, J. T., G. Münch, and F. L. Roesler (1980). A study of the Jovian [SII] nebula at high spectral resolution. Astrophys. J., 236, 1035-1042.

Trauger, J. T., and F. L. Roesler, (1972). Appl. Optics, 11, 1964.

York, D. G., E. B. Jenkins, P. Zucchino, J. L. Lowrance, D. Long, and A. Songaila (1981). Proceedings of SPIE, eds. J. C. Geary and D. W. Latham, 290, 202.

TABLE I

INSTRUMENTAL PASSBANDS

	February (A)	March (A)
Interference Filter[a]		
[S II] λ6716	12.8	12.8
[S II] λ6731	15.8	15.8
[S III] λ9531	17.5	17.5
Fabry-Perot		
[S II] λ6716	1.8	1.0
[S II] λ6731	1.8	1.0
[S III] λ9531	4.1	1.7

[a]Narrow-band interference filter isolated a selected transmission peak of the Fabry-Perot.

TABLE II

LOG OF FABRY-PEROT/CCD OBSERVATIONS

Date (1981)	Time[1] (UT)	Emission[2] Line	λ_{III}(FOV)[3] (deg)	Aspect[4] (deg)	Intensity[5] (R)	λ_{III}(Io)[6] (deg)	Quality[7] Factor
Feb 16							
	7:31	[S II]b	236	-6.9	115	90	1
	8:15	[S III]	263	-9.0	230	111	1
	8:52	[S II]a	286	-9.7	80	129	1
	9:25	[S II]a	305	-9.5	70	143	1
	10:34	[S III]	347	-6.5	315	167	1
	11:18	[S II]a	14	-3.4	100	196	1
	11:59	[S III]	38	-0.4	375	214	1
	12:28	[S III]	56	1.5	420	228	1
	12:42	[S III]	65	2.4	455	235	1
Mar 25							
	5:42	[S II]a	345	-6.7	105	241	3
	6:00	[S II]b	356	-5.5	130	250	3
	7:55	[S II]b	66	2.4	145	303	3
	8:36	[S II]a	90	4.0	150	322	3
	10:41	[S III]	166	1.3	635	20	2
	11:00	[S II]b	178	0.1	350	29	2

Table II (cont.)

Mar 26						
7:50	[S II]b	33	-4.3	95	248	3
8:47	[S II]a	68	-7.9	110	274	3
9:13	[S II]b	83	-9.0	85	286	3
10:37	[S II]b	134	-9.1	165	325	3
11:09	[S II]a	154	-7.8	165	37	3

[1]Universal time at beginning of observation. All observations were 10 minutes, except the 20 minute observations taken at 11:18 on February 16 and at 7:50 on March 26.

[2][S II]a λ6716; [S II]b λ6731; [S III] λ9531

[3]System III magnetic longitude (1965.0) of the FOV in the plane of the sky at the midpoint of the observation. All observations were taken west of Jupiter, except for the east [S II] images taken on March 26.

[4]Jovicentric centrifugal latitude of the Earth.

[5]Peak surface brightness (1 Rayleigh = $10^6/4\pi$ photons cm^{-2} sr^{-1}).

[6]Mean magnetic longitude of Io.

[7]The degree to which systematic errors in determining the Fabry-Perot transmission correction would affect the derived intensity distribution: (1) no significant changes; (2) slight changes; (3) significant changes.

TABLE III

FP/CCD OBSERVATIONS: SCALE HEIGHTS

		Scale Height[a]	Ion Temperature (10^3 K)[b]	
		(R_J)	($m_i^* = m_i$)	($T_i = T_e$)
March 1980[c]	S II	0.27±.01	66±5	33±2
	S III	0.86±.06	670±95	225±35
February 1981	S II	0.72±.04	470±70	235±35
	S III	0.73±.03	485±40	160±15
March 1981	S II	0.58±.06	305±65	155±35
	S III	0.62±.04	350±45	115±15

[a]Scale height measured along magnetic field lines for 'edge-on' images. The scale height is for the warm torus ($L \geq 5.8$ R_J), except for the 1980 March [S II] which is in the cold torus.

[b]The ion temperature was calculated under different assumptions about the effective ion mass (see text).

[c]For [S II] ϕ=1.6° and for [S III] ϕ=-3.9° (Roesler et al. 1982).

TABLE IV

RESULTS OF [S II] λ6731 EMISSION LINE SCANS

Scan Number	Time (UT)[a]	r (R_J)[b]	λ_{III}^{FOV} (deg)	Line Center (km/s)[c]	V_{cr} (km/s)[d]	Temperature (10^3 K)	Intensity (Rayleighs)[e]
1	7:57	6.0	40	...	-74.3	...	...[f]
2	8:23	5.2	56	-61.7±0.7	-64.3	67±18	210±25
3	8:47	5.2	71	-61.4±0.8	-64.4	41±17	160±20
4	9:17	5.4	89	-64.5±0.9	-67.5	48±23	140±20
5	9:40	5.6	103	-67.2±0.7	-70.0	50±17	230±30

[a]Date of observations: 1981 March 26

[b]Distance from Jupiter with 0.8 R_J FOV centered 2.5°-4.9° north of the centrifugal equator (see Fig. 4).

[c]Doppler-shifted velocity with respect to Jupiter (corrected for Earth's rotation and Earth-Jupiter radial motion).

[d]Predicted corotational velocity

[e]1 Rayleigh = $10^6/4\pi$ photons cm^{-2} s^{-1} sr^{-1}

[f]No emission was detected (see text).

Figure Captions

Figure 1. Examples of [S II] λ6731 and [S III] λ9531 raw emission line frames ((a) and (c)) and their corresponding continuum frames ((b) and (d)). The + symbol marks the center of Jupiter. The saturated images of the Galilean satellites, Europa (E) and Ganymede (G), and several internal reflections are present in the [S II] sequence. Several, but not all, of the internal reflections (r) and cosmic ray hits (cr) are noted. The vertical stripe in column 41 is due to an 'overflow' from several 'hot' pixels near the top of that column. The edge of the occulting mask produced the long linear feature on the left. The contour levels for the [S II] sequence are 100, 200, 300, 400, 500, 600, 700, 800, 900, 1900, and 2900 data numbers. The contour levels for the [S III] sequence are 50, 100, 150, 200, 250, 300, 350, and 400 data numbers.

Figure 2. Examples of Fabry-Perot transmission corrections (dashed lines) superimposed on their respective [S II] and [S III] final processed images (solid lines); the raw data was shown in Fig. 1. Europa is on the eastern edge of the [S II] emission. For purposes of presentation, the final processed images were rotated and shifted to align the Jovian centers and to locate the predicted position of the centrifugal equator along the same row. Distances from Jupiter with a negative sign refers to the directions south or east in the centrifugal frame of reference. Furthermore, the images were median filtered to reduce the noise levels enhancements caused by the Fabry-Perot correction. The contour levels are 12.5, 25, 50, 75, and 100 Rayleighs for [S II], and 37.5, 75, 150, 225 and 300 Rayleighs for [S III].

Figure 3. The torus [S II] λ6731 emission line measured with the high-resolution Fabry-Perot spectrometer. The scan details are given in Table IV and the exact locations of the FOVs with respect to the [S II] emission are shown in Fig. 4. The background scan was taken 5.6 R_J and 44° southeast of the Jovian center. The scans are aligned such that V=0 km/s corresponds to the predicted corotational velocity for the center of the FOV. The model fit to the data (solid line) is a single Gaussian with a linear background convolved with the instrumental profile. The instrumental profile was determined from scans of a thorium I (λ6729.9325) line and positioned at v=0 km/s for comparison.

Figure 4. The 0.8 R_J FOV of the 4 meter Fabry-Perot scanning spectrometer superimposed on the 2.1 meter [S II] FP/CCD images. Scans 1, 2, 3, 4, and 5 were positioned at 6.0, 5.2, 5.2, 5.4, and 5.6 R_J from Jupiter, respectively. Scans 2 and 5 were taken approximately midway between two [S II] images; thus their FOVs are each plotted (dashed circles) on the image taken before and after their respective scans. For purposes of presentation, the final processed images were rotated and shifted to align the Jovian centers and locate the predicted positions of the centrifugal equator along the same row. The images were also median filtered. The open contour lines are areas excluded from analysis due to Fabry-Perot transmission decreasing to <0.3 (see data reduction section). The contour levels are 12.5, 25, 50, 75, 100, 150 and 200 Rayleighs.

Figure 5. Examples of [S II] (left) and [S III] (right) final processed images. For presentation purposes, these images were rotated and shifted to align the Jovian centers and locate the predicted position of the centrifugal equator along the same row. Furthermore, each image was median filtered. The contour levels for the [S II] images are 12.5, 25, 50, 75, 100, 150, 200, and 300 Rayleighs. The contour levels for the [S III] images are 37.5, 75, 150, 225, 300, 450 and 600 Rayleighs. ϕ = Jovicentric centrifugal latitude of the Earth or the torus aspect.

Figure 6. The position of the peak intensity (solid symbols) and the maximum detectable radial extent (open symbols) of emission along the centrifugal equator versus magnetic longitude. Torus data from Roesler et al. (1982) is included for comparison. For visual aid, observations taken on the same night are connected together by long dashes (peak) or short dashes (radial extent).

Figure 7. A sequence of single Gaussian fits to the observed [S III] intensity distribution along the magnetic field line (0 = predicted position of centrifugal equator). $\lambda_{III}=56^\circ$ and $\phi=1.5^\circ$.

Figure 8. The fitted scale heights of the intensity distributions along the magnetic field lines as measured from approximately 'edge-on' images (see text). The formal 1σ errors from the Gaussian fit are ~0.02-0.04 R_J. Torus data from Roesler et al. 1982 has been further analyzed and is included for comparison in (a).

Figure 9. Contours (dashed lines) of the warm torus model fitted to a [S III] image. The [S III] image was rotated to align the centrifugal equator along a row for comparison with the model. This processed image is not median filtered (compare to Fig. 2b, noting that the contour levels are slightly different). The contour levels are 47, 94, 141, 188, 282, and 376 Rayleighs.

Figure 1

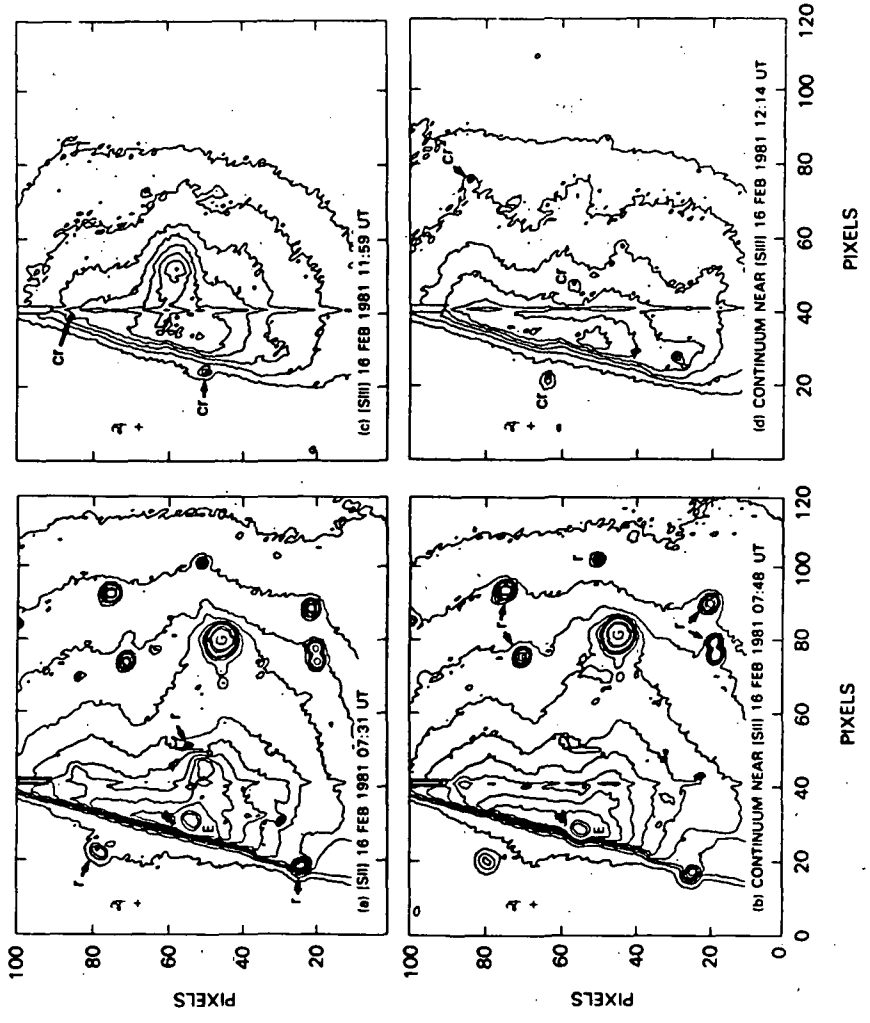

Figure 2

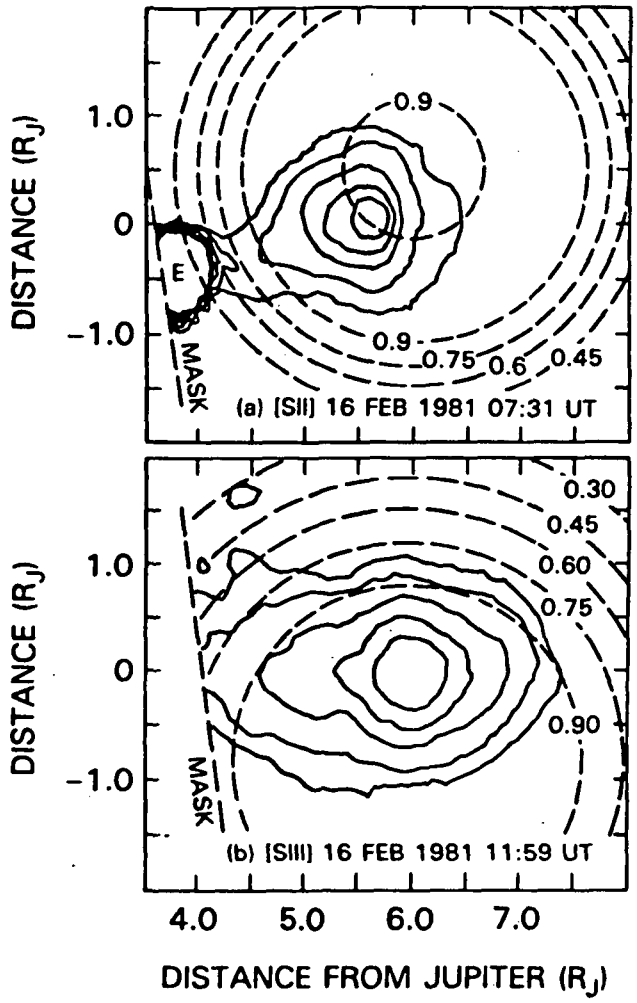

Figure 3

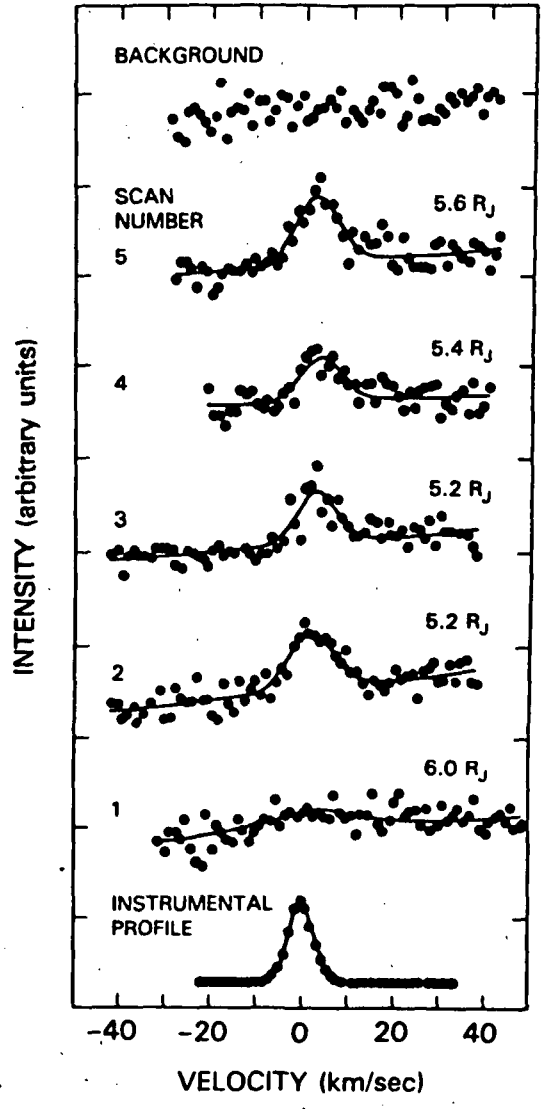

Figure 4

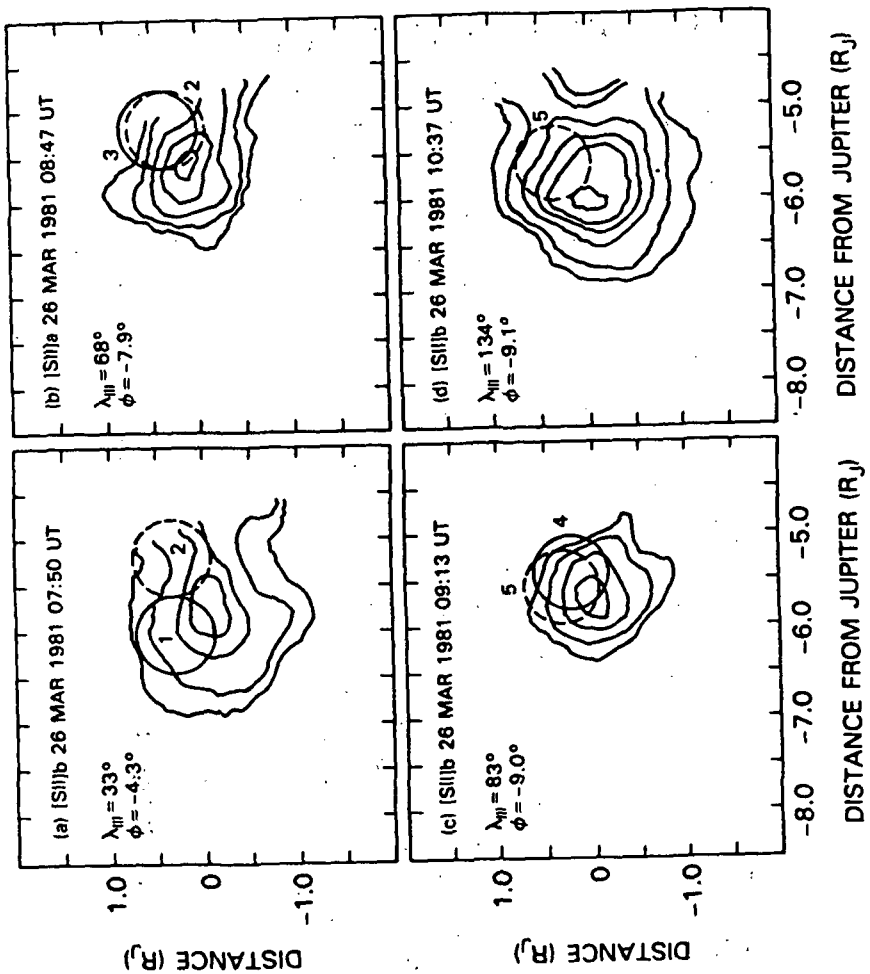

Figure 5

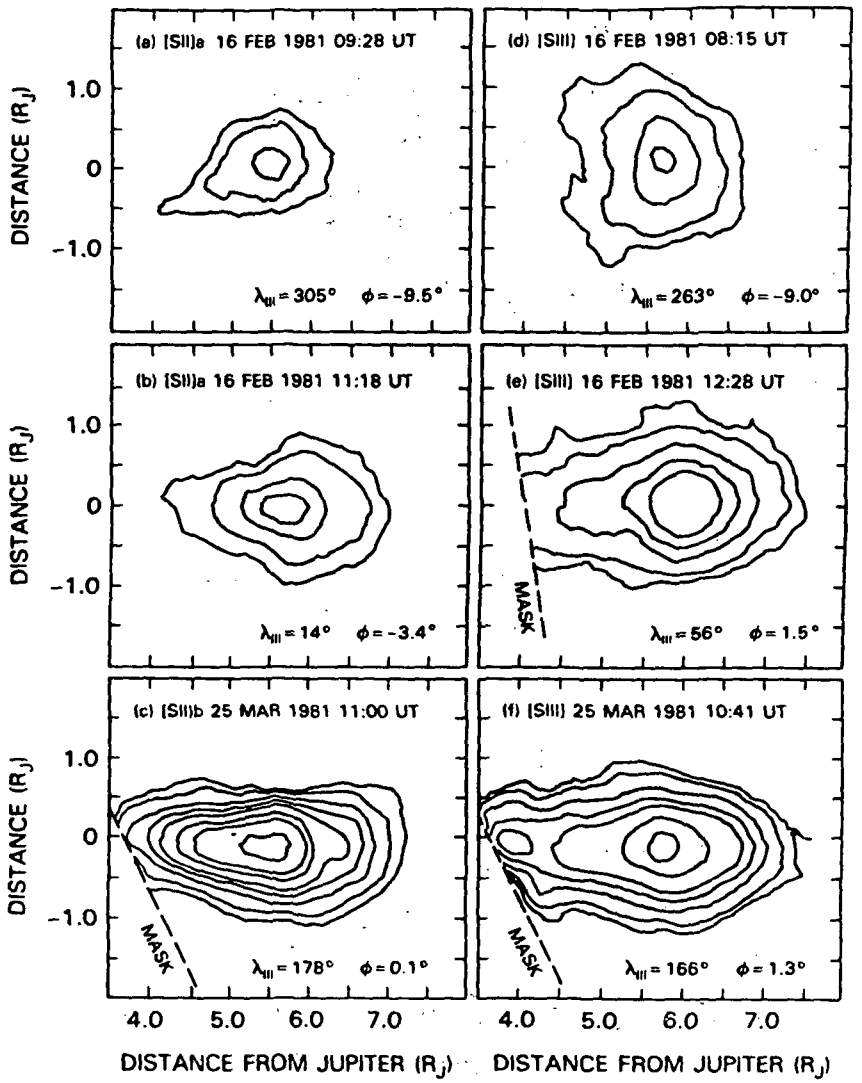

Figure 6

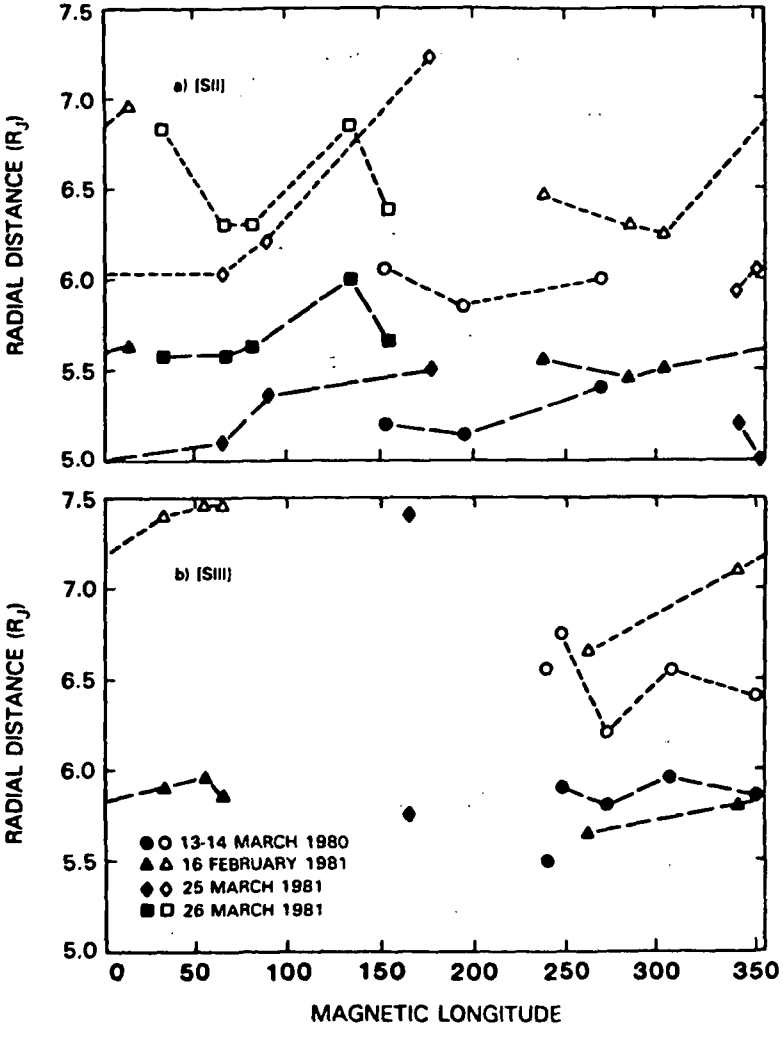

Figure 7

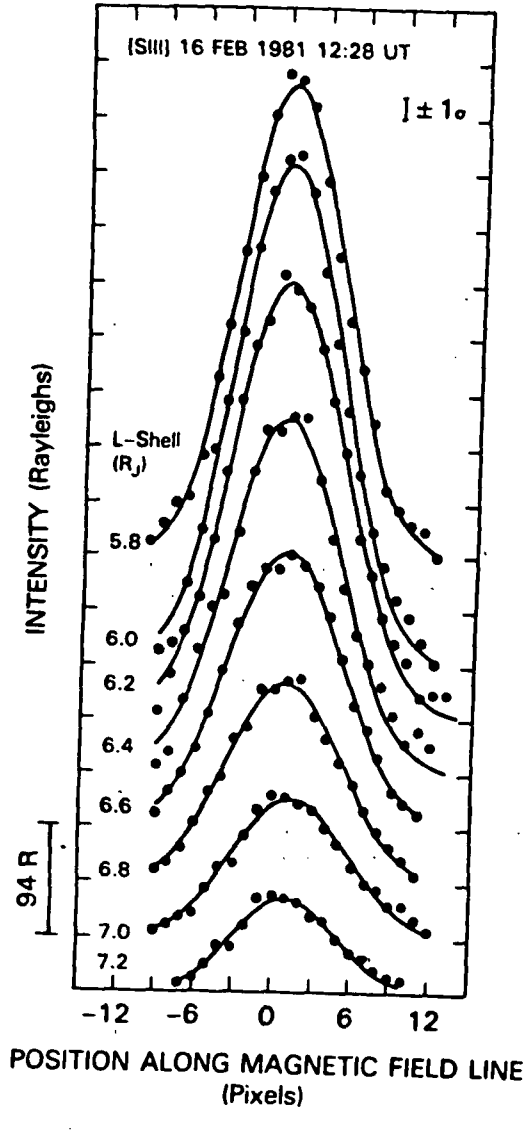

Figure 8

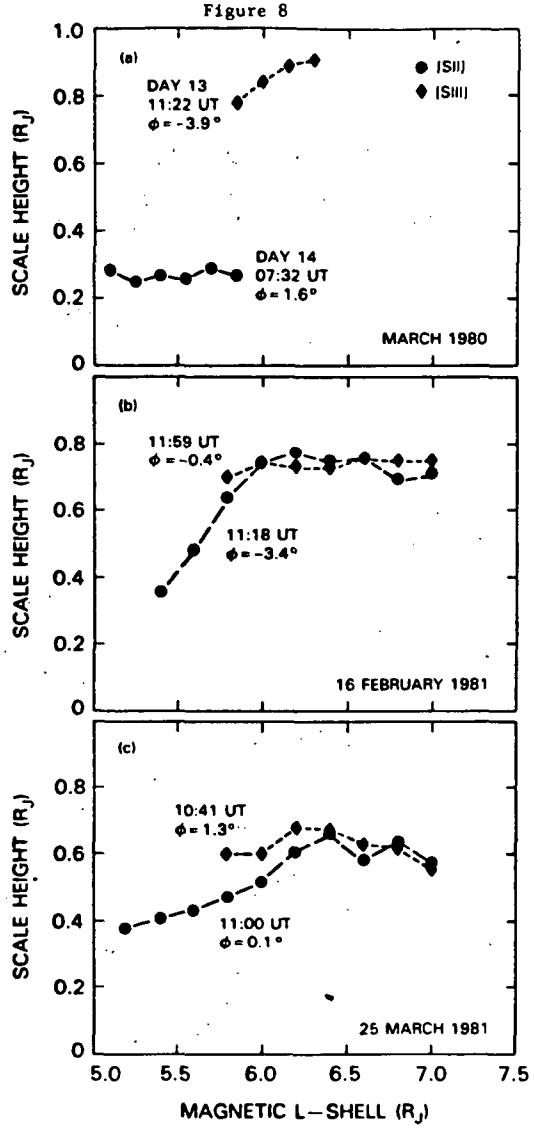

Figure 9